Angiography with a multifunctional line scanning ophthalmoscope

Daniel X. Hammer
R. Daniel Ferguson
Ankit H. Patel
Vanessa Vazquez
Deeba Husain

Angiography with a multifunctional line scanning ophthalmoscope

Daniel X. Hammer,[a] **R. Daniel Ferguson,**[a] **Ankit H. Patel,**[a] **Vanessa Vazquez,**[b] **and Deeba Husain**[b]
[a]Physical Sciences Inc., 20 New England Business Center, Andover, Massachusetts 01810
[b]Boston University School of Medicine, Department of Ophthalmology, Boston, Massachusetts 02114

Abstract. A multifunctional line scanning ophthalmoscope (mLSO) was designed, constructed, and tested on human subjects. The mLSO could sequentially acquire wide-field, confocal, near-infrared reflectance, fluorescein angiography (FA), and indocyanine green angiography (ICGA) retinal images. The system also included a retinal tracker (RT) and a photodynamic therapy laser treatment port. The mLSO was tested in a pilot clinical study on human subjects with and without retinal disease. The instrument exhibited robust retinal tracking and high-contrast line scanning imaging. The FA and ICGA angiograms showed a similar appearance of hyper- and hypo-pigmented disease features and a nearly equivalent resolution of fine capillaries compared to a commercial flood-illumination fundus imager. An mLSO-based platform will enable researchers and clinicians to image human and animal eyes with a variety of modalities and deliver therapeutic beams from a single automated interface. This approach has the potential to improve patient comfort and reduce imaging session times, allowing clinicians to better diagnose, plan, and conduct patient procedures with improved outcomes. © *2012 Society of Photo-Optical Instrumentation Engineers (SPIE).* [DOI: 10.1117/1.JBO.17.2.026008]

1 Introduction

Severe loss of vision can occur from the growth of abnormal choroidal blood vessels that invade the retinal pigment epithelium (RPE) and photoreceptors through Bruch's membrane. This angiogenesis, also called subretinal neovascular membranes (SRNM), can result from diseases, such as age-related macular degeneration (AMD), choroiditis, and myopic retinopathy, or from acute trauma and laser injury. The current standard treatment for this condition is an intravitreal injection of anti-vascular endothelial growth factor (VEGF), such as Lucentis or Avastin.[1,2] Other treatment modalities include laser surgeries, such as photodynamic therapy (PDT).[3] Combined strategies that effectively employ both methods are also being explored.[4,5] PDT acts by selective dye accumulation, activation by laser light, and disruption and clotting of the new leaky vessels. Current strategies predominantly rely on fluorescein angiography for diagnosis but rarely use imaging to guide laser surgical treatment or drug injection. Although PDT surgery is infrequently performed because of the success of anti-VEGF drug therapies, many subjects still select this option due to aversion to intravitreal injections. In general, laser surgery remains the only treatment option for many eye diseases.

Indocyanine green angiography (ICGA) and fluorescein angiography (FA) are usually used to identify specific areas of blood vessel leakage in the choriocapillaris and retinal vasculature. Fluorescein absorbs in the 485 to 490 nm wavelength range and emits at ~530 nm and so is useful for visualization of retinal vasculature in front of the highly pigmented RPE layer.

Unbound sodium fluorescein is contained in the retinal vasculature by their tight junctions but diffuses through choriocapillaris vessels.[6] ICG is excited and fluoresces at longer wavelengths in the near infrared (805 and 835 nm) and so these more deeply penetrating wavelengths are useful for visualization of choroidal circulation. ICG also has a higher molecular weight and binds nearly completely to plasma proteins and so the dye leakage, and hence available imaging time, is longer.

Angiography and laser surgery are rarely accomplished on the same instrument or even in the same session. Laser retinal surgery is also not typically image-guided and is often conducted using a contact lens and slit lamp. Some recently offered clinical devices (e.g., OS/OD Navilas) have made strides toward the integration of imaging and treatment hardware for the planning and execution of customized laser surgery.

We have developed a multifunctional platform for automated ophthalmic diagnosis and therapy. Our approach was to enhance a tracking scanning laser ophthalmoscope (TSLO) with hardware for angiography and treatment beam delivery. The TSLO combines retinal tracking (RT)[7–12] and line scanning ophthalmoscopy (LSO)[13] techniques into a single compact instrument for wide-field confocal retinal imaging and stabilization of image/stimulus/treatment beams through all lateral eye movements. The TSLO has proven effective in applications such as retinal hemodynamics Doppler flowmetry and 3-D OCT that suffer from eye motion artifacts.[14,15] The LSO is a unique confocal imager with only one moving part, allowing for simplified optics and a compact footprint. The new clinical prototype system, which includes LSO imaging in NIR confocal reflectance, FA, and ICGA modes, RT, and PDT laser delivery is called the multifunctional line scanning ophthalmoscope

Address all correspondence to: Daniel X. Hammer, Physical Sciences Inc., 20 New England Business Center, Andover, Massachusetts 01810. Tel: 978-738-8224; Fax: 978-689-3232; E-mail: hammer@psicorp.com.
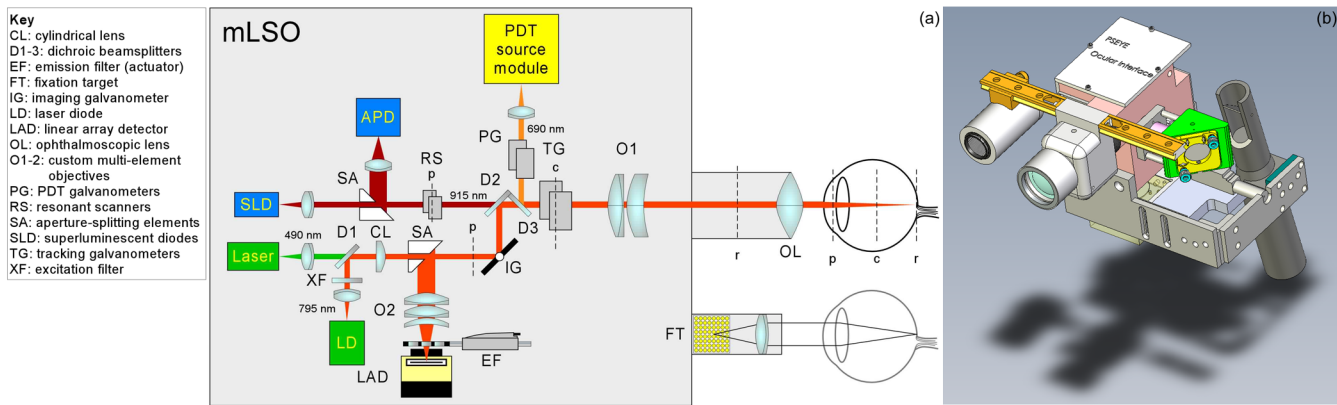
(mLSO). A functional block diagram of the mLSO system is shown in Fig. 1. The mLSO was tested in fundamental imaging modes (LSO and RT) in human eyes without disease. The fluorescence imaging channels were tested in a pilot clinical trial on subjects with a variety of retinal diseases that are normally imaged with angiography.

In addition to the mLSO hardware, we have also developed new automated clinical procedures for treatment of SNRMs. The procedures allow a surgeon to rapidly diagnose and treat lesions from a single platform, which uses image guidance for various laser- or drug-based interventions. The system also employs new techniques and software for unique presentation and quantification of diagnostic information.

Line field or line scanning angiography (LSA) is a new imaging technique that has been demonstrated in the proof-of-principle studies described in this paper. It offers an alternative with certain advantages and disadvantages compared to traditional retinal imaging techniques, particularly confocal SLO angiography and non-confocal fundus photography. For example, LSA can attain higher frame rates and resolution than an SLO, which may be important for some research applications that involve dynamic events. With less complexity, the hardware also has the potential for improved compactness, including hand-held designs for applications with space constraints.

The depth-sectioning light collection efficiency is similar to an SLO, which can be an advantage or disadvantage in terms of image appearance. New hardware designs (e.g., linear detectors with asymmetric pixels) enhance light collection. LSA thus provides an alternative technical approach that can be adopted when the application warrants.

2 Materials and Methods

2.1 mLSO System

The mLSO retinal imaging and treatment system was designed around PSI's core tracking scanning laser ophthalmoscope (TSLO) technology,[7,8] which includes retinal tracking (RT) and line scanning ophthalmoscope (LSO) hardware. A schematic and SolidWorks opto-mechanical model of the optical head is shown in Fig. 2. The active retinal tracking works by directing a low power beam at a target in the retina (usually the optic nerve head) to detect and compensate for eye movements.[7–9] The tracking beam is dithered at a high frequency (16 kHz) with resonant scanners and detected with a confocal reflectometer. The resultant signal is phase processed to generate x- and y-error signals, which are fed into the closed-loop galvanometers to stabilize the imaging and PDT beams

Fig. 1 Conceptual block diagram of the mLSO system. The system includes a confocal LSO imager configured for angiography (490-nm and 795-nm excitation), a retinal tracker (915 nm), and a PDT treatment laser (690-nm beam) delivered through tracking scanners to fixed retinal coordinates. The system continuously provides high-contrast images of the fundus to monitor PDT laser spot and eye position data during any imaging or therapeutic procedure.

Fig. 2 Schematic (a) and opto-mechanical model (b) of the mLSO optical head.

on fixed retinal coordinates through all eye motion. The retinal tracker hardware includes a phase-locked resonant scanner pair and the optics that constitute the confocal reflectometer. The LSO is a quasi-confocal, line-scanning, wide-field retinal imaging platform.[13] The LSO hardware includes a cylindrical lens (CL), a single scanning galvanometer, and a linear array detector (LAD, e2v Inc.). The imaging optics consist of custom objectives (O1: scan objective, O2: detector objective) and a front ophthalmoscopic lens (OL). The instrument can be configured with several different ophthalmoscopic lenses (e.g., Volk 40D, 66D, 78D) to achieve a variety of retinal field sizes.

To the core TSLO hardware, we have made four additions to enable multifunctional capabilities. First, a compact visible (490-nm) laser and coupling optics (filters, fiber-couplers) were added to the instrumentation for fluorescein excitation. Second, an illumination port was added to the optical head to couple the fluorescein excitation laser beam into the optical beam path. Third, a computer-controlled, motorized filter stage was inserted in front of the camera to switch rapidly between reflectance, ICGA, and FA modes for interleaved operation and display. Fourth, a treatment beam port was added for a commercial off-the-shelf PDT laser.

The mLSO has been configured with sources, filters, and dichroic beamsplitters specifically to collect near-infrared confocal reflectance images and ICG and fluorescein angiograms. A low-pass (∼600 nm cutoff) dichroic beamsplitter (D1) directs the 490-nm laser source used for FA into the optical path. A high-pass (∼900 nm cutoff) dichroic beamsplitter (D2) combines the tracking and imaging beams. A custom band-pass filter (Omega Optical Inc.) at 690 nm (D3) directs the PDT laser into the optical path. The Zemax optical design showed good performance of the optics at both 490 and 795 nm.

Two illumination beams are combined into the main imaging path: the near infrared (795 nm) light for confocal reflectance imaging and ICG angiography, and the 490-nm light for fluorescein angiography. A superluminescent diode (SLD) with 760-nm center wavelength (Exalos Inc.) was also used in place of the 795-nm LD source to generate some LSO images. SLDs produce images with less speckle noise, but no SLDs are currently available at the ICG excitation peak. An excitation filter (751 to 798 nm) prevented illumination light from reflecting back into the detector in the ICG emission band. The 490-nm laser source (Cobolt Calypso laser) is an extremely compact laser with an output power of ∼25 mW. A collimator affixed to a tip-tilt mirror mount is used to couple the light into a single-mode fiber

connected to the optical head. Fixed neutral density filters prevent light exposure to the patient above the ANSI safety limits. The system uses a 915-nm superluminescent diode (SLD) for retinal tracking.

The PDT laser added to the system is manufactured by Carl Zeiss Meditec Inc. (Visulas 690 s and Visulink PDT/U) and has an output wavelength of 690 nm. The laser is designed to be mounted on several different manufacturers' slit lamps. The PDT laser consists of a control box, an optical port, and a foot switch. The controller has a touch screen to allow the user to change parameters such as light dose and exposure time.

A filter stage was designed to switch rapidly between emission filters (EF) for reflectance, ICGA, and FA using a Quick-shaft linear actuator (Faulhaber). The actuator has a top speed of 1.9 m/s and uses Hall sensors to achieve a resolution of 6 μm, a repeatability of 40 μm, and a precision of 120 μm over the positioning range. Three filter slots house emission filters for ICGA and FA and Schott glass for confocal reflectance LSO imaging. The FA emission filter passes visible light from 507 to 562 nm, and the ICGA emission filter passes NIR light from 819 to 863 nm. The filters were made the same optical thickness to prevent path length differences that would affect image focus when switching filters. The linear actuator is driven by commands from the PC (serial interface) with a small motion controller board integrated into the instrumentation box. In addition to switching emission filters, an FA illumination source shutter assembly is also mounted to the actuator so that when the filter stage is in any position other than FA, it will block the 490-nm laser beam from entering the eye.

The mLSO also includes an integrated LED-array fixation target (fellow-eye) and the PDT laser delivery component. Fellow-eye fixation may introduce eye position errors, but the fixation target is only intended to coarsely position the subject's gaze direction to lock and re-lock tracking on particular targets.

The final design for the optical head includes the dual illumination port, which fits entirely within the external enclosure of the standard TSLO optical head, the Maxwellian PDT port, which includes relay optics (lens and turning mirror), galvanometer-driven mirrors to position the PDT beam anywhere on the retina, and the Zeiss PDT laser mounted to the side of the optical head, and the angiography filter sub-assembly, composed of the linear actuator and the filter slide mounted to the same bracket used to mount the PDT laser.

All system electronics and instrumentation are contained in a single instrumentation box. The instrumentation box and system
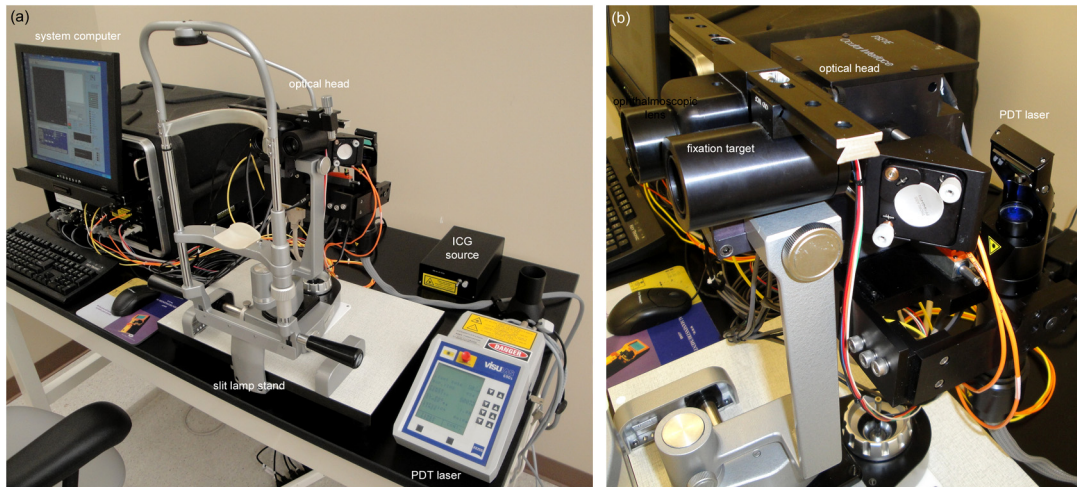
Fig. 3 Photograph of mLSO system. (a) Complete system. (b) Optical head.

computer are housed in a compact 19-inch rack. The electronics are built around two custom-printed circuit boards and a motherboard and field programmable gated array (FPGA)-based tracker controller board; they also include several commercial OEM driver electronics boards. The primary function of the tracker controller board is to run the feedback loop independently between the detector and galvanometers in real time.

The motherboard has hardware to interface with the OEM driver boards for the galvanometers (Cambridge Technology), resonant scanners (EOPC Inc.), and laser diodes and SLD sources (Exalos and QPhotonics). It also includes integrated LD/SLD thermo-electric coolers and drivers, integrated custom silicon detector electronics (for the tracking reflectometer), power regulation electronics, and header slots to mount and communicate with the custom retinal tracker control board. The tracker control electronics are composed of two boards: a Xilinx Virtex-4 FPGA mini-module board and an analog front-end (AFE) that includes a six-channel 250-kHz analog-to-digital converter (ADC), a four-channel, 100-kHz digital-to-analog converter (DAC), digital input/output (DI/O) lines, and serial communication with the host PC. The detector signal is sampled at 208 kHz, and the eye position data are transferred to a PC at a decimated rate of 1 kHz. Photographs of the mLSO system and optical head are shown in Fig. 3. Key specifications for the mLSO components are highlighted in Table 1.

2.2 Subjects

The mLSO system was tested in two human subject studies. The first, performed at PSI, was on a small number of subjects without retinal diseases ($n = 3$) to validate, characterize, and optimize LSO imaging and retinal tracking. The second, performed at Boston University Medical Center (BUMC), was a pilot clinical investigation on 10 subjects with retinal disease and one without retinal disease. The BUMC study was designed to demonstrate line scanning angiography. The diseases examined included diabetic retinopathy (DR, with macula edema), central serous chorioretinopathy (CSC), sickle cell retinopathy, and a possible case of macular degeneration. IRB protocols were submitted and approved by New England IRB for the initial PSI study and the BUMC IRB for the pilot clinical study. All subjects gave informed consent prior to imaging.

Table 1 Key specifications for mLSO components.

Component	Specification	Value
LSO	Wavelength	795 nm (760 nm)
	Image size (at retina)	~13.9 × 13.9 mm (~48 × 48 deg)
	Image size	1024 × 1024 pixels
	Pixel size (at retina)	13.6 μm
	Frame rate	15 to 60 fps
FA	Excitation wavelength	490 nm
	Emission wavelength	507 to 562 nm
ICGA	Excitation wavelength	795 nm
	Emission wavelength	819 to 863 nm
PDT	Wavelength	690 nm
	Beam size (at retina)	0.8 to 4.9 mm (2.7 to 16.8 deg)
RT	Wavelength	915 nm
	Closed loop bandwidth	>1 kHz (limited by galvos)
	Tracking accuracy	~15 μm RMS

2.3 Imaging Protocol

For the PSI study, LSO images were acquired, and the system optics were aligned. No angiography was performed, but artificial fluorescent targets were used to verify operation of the FA and ICGA modes prior to the BUMC study. For validation and optimization of retinal tracking, the subjects were asked to gaze at the illuminated light on the LED array (spacing ~2.5 deg.) during a patterned illumination sequence while tracking was active. The performance of the automatic blink/re-lock algorithm was also verified.

The BUMC pilot clinical study was designed to perform complementary imaging on patients undergoing standard fundus camera angiography to verify mLSO performance. The mLSO system was set up in the clinical space immediately adjacent to a TopCon Fundus Photography System (model #TRC50X). Initial clinical testing at BUMC was limited to verification and optimization of the angiography imaging modes alone. For the subject without retinal disease and the subject with CSC, we obtained FA and ICGA sequences during the initial dye-infusion stage. In all other patients, the subjects were first imaged on the TopCon system during dye injection and then moved over to the mLSO after a few minutes. This procedure somewhat limited the visualization of early stage dye infusion, when the dye concentration is largest; however, it did not hinder resolution of late stage leakage.

The mLSO was configured to acquire FA and ICGA images at 1 frame per second (fps). The power at the cornea was ~0.6 mW and ~1 mW for the individual FA (490 nm) and ICGA (795 nm) sources, which were not used simultaneously. Because the 490-nm source is extremely bright to the patient, we configured the mLSO imager to modulate this source by collecting three frames at 490 nm, followed by seven LSO frames for every 10 frames acquired. The NIR LSO beam power was reduced to $<50-100$ μW for the longer integration time that accompanied the lower frame rate (the LSO is typically run at 15 to 60 fps). The software was configured to switch automatically between appropriate bandpass filters, trigger the ICGA shutter, and change to image brightness scaling to accommodate the different FA and LSO reflectance modes during acquisition of this sequence. For ICGA, the videos were acquired continuously.

Because the mLSO and the TopCon always imaged an eye at different time points with respect to the dye infusion, a direct comparison between the two devices was not possible. Nonetheless, we were able to move some subjects fast enough between instruments to get a general idea of the appearance of early and late phase angiograms on both instruments. Also, while we do make a comparison in the results that follow, the principal aim of the investigation was to demonstrate the feasibility of line scanning angiography and not to compare it to current clinical techniques.

3 Results

3.1 LSO Imaging

Preliminary system characterization was performed on artificial targets and resolution charts. The wide-field imager had good flatness across the field. Over the ~48-deg field (13.9 mm), the system can resolve objects with a resolution of ~15 μm (image pixel size = 13.5 μm referenced to the retina). The PDT beam power measurements also verified expected losses through the system of ~25%. The adjustment range for the PDT beam diameter is 0.8 to 4.9 mm. The spot size measurements resulted in an average error across this range of ~3.5%, indicating proper beam alignment and relay lens positioning.

The initial human subject testing also showed good preliminary results in terms of imaging performance and retinal tracking. A comparison of single and composite averaged images with and without tracking for one subject are shown in Fig. 4. The LSO images are nearly equivalent to flying-spot confocal images in terms of contrast, reduced scatter, and depth sectioning. Because this subject was a good fixator, even the non-tracking composite image [Fig. 4(c)] shows coarse retinal features. However, in terms of the resolution of fine features (see inset of Fig. 4), such as capillaries around the foveal avascular zone (FAZ), the tracking composite image [Fig. 4(b)] has nearly the same appearance as the single frame [Fig. 4(a)]. In contrast, features are doubled and blurred in the non-tracking average.

3.2 Retinal Tracking

Retinal tracking in two subjects during eye movement tasks is shown in Fig. 5. The composite (i.e., averaged) image and corresponding eye movement positions are shown. The accompanying videos (Videos 1 and 2) show real-time dynamic tracking during the tasks. Retinal tracking was robust on the small number of subjects tested. Tracking performance was similar to other recent reports.[10–12]

3.3 Line Scanning Angiography

In the results that follow, the images from the mLSO are presented, along with images from the TopCon system. We tried to choose frames that were nearly equivalent in terms of dye infusion times, but as mentioned above, this was often difficult because the subjects were imaged at different times on each device. The optical resolution of the TopCon is better than the present mLSO e2v line-camera implementation (1024×1024 pixels versus 1900×1472 across a similar field size), which should be considered in comparing the images presented. The mLSO can be designed to accommodate higher pixel density.

The subject without retinal disease was imaged first on the mLSO and then on the TopCon with both FA and ICGA. The
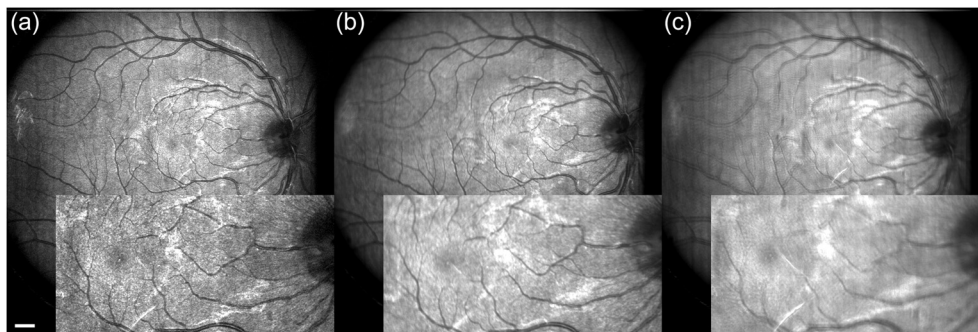

Fig. 4 mLSO imaging and tracking performance for one PSI subject (male, normal vision, age 25, excellent fixator). (a) Single LSO frame. (b) 50 frames (>3 sec.) with tracking. (c) 50 frames without tracking. Inset for each show 2× magnification of region between fovea and ONH. Foveal pit, nerve fibers, and small capillaries around FAZ are clear in single and tracked frame but blurred in non-tracked frame. Bright reflections near the macula and ONH are from nerve fiber layer. Scale bar = 3 deg.
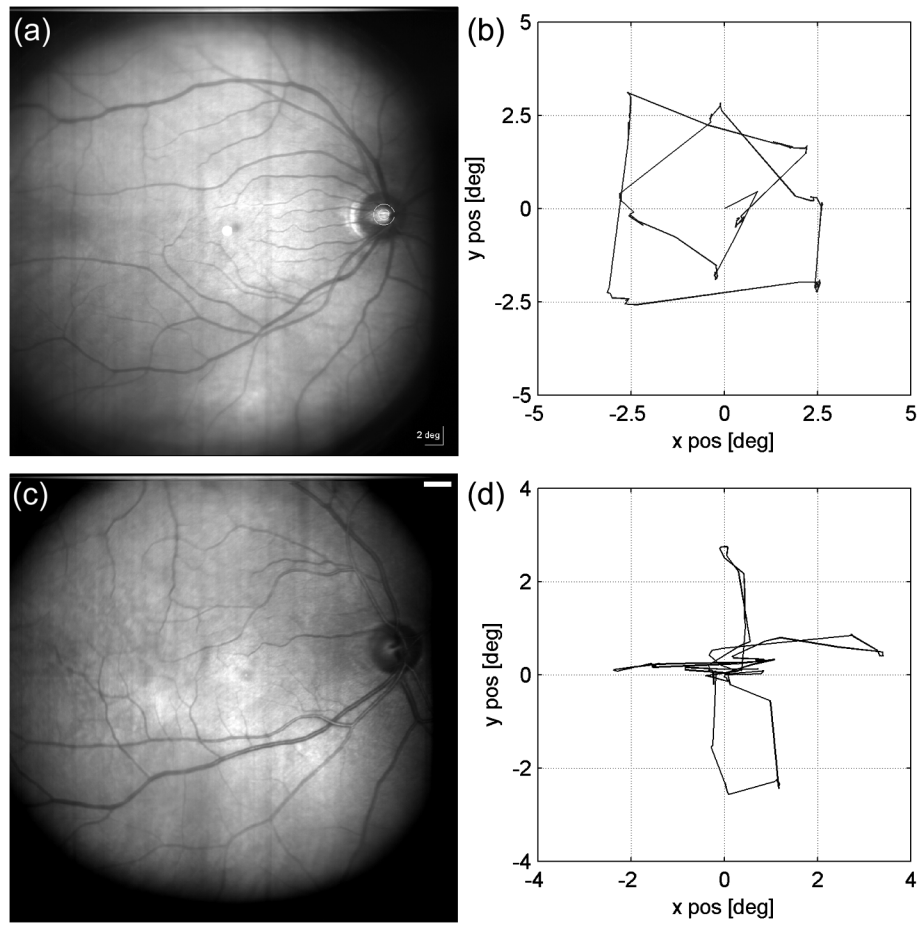
Fig. 5 Retinal tracking performance for eye movement tasks in two PSI subjects. Shown are composite averages (a) and (c) and eye movement charts (b) and (d). Subjects were asked to gaze at patterned illuminated fixation targets with spacing of ∼2.5 deg during tracking. (a) Composite image generated from 142 video frames (∼10 sec) acquired during eye movement sequence for subject 1. Overlay shows display as viewed in the acquisition software with tracking beam position in the ONH, fixation target position, and 2-deg scale bar. (b) Eye position data for box/diamond task. (Video 1, MOV, Quicktime, 6.0 MB) [URL: http://dx.doi.org/10.1117/1.JBO.17.2.026008.1]. (c) Composite images generated from 166 video frames (∼11 s) acquired during eye movement sequence for subject 2. (d) Eye position data for cross task. (Video 2, MOV, Quicktime, 7.1 MB) [URL: http://dx.doi.org/10.1117/1.JBO.17.2.026008.2]. Scale bar in (c) =3 deg. Subject 1: 38-year-old male with –7D of myopia, imaged with contacts. Subject 2: 49-year-old emmetropic and presbyopic male.

results are shown in Fig. 6. The upper row shows the TopCon images, and the lower row consists of the mLSO images. The TopCon images include a red-free image (a), a late phase FA (b), and a late phase ICGA (c). The mLSO images include the NIR reflectance image (d), an early phase FA (e), and an early phase ICGA (f). Videos 3 and 4 show the accompanying FA video (at 15 fps). Video 3 shows the raw FA image acquisition with LSO and FA images interleaved. Video 4 shows the FA images extracted from Video 3. The mLSO FA image shows good resolution of all the retinal vasculature. As a consequence of the mLSO confocality, the choroidal vessels in the FA image are not as visible as in the TopCon. However, the mLSO ICGA image shows good contrast of the choroidal vessels.

The subject with central serous chorioretinopathy (CSC) was imaged first on the mLSO and then on the TopCon with both FA and ICGA. The results are shown in Fig. 7 with a similar arrangement of panels as Fig. 6. Video 5 shows the accompanying ICGA video (at 15 fps). In this subject, the area of the disease is clear in the FA images, with hyper-fluorescence in lesions immediately adjacent to the disc on the temporal side. The ICGA images show good contrast and hypo-fluorescence in the choroidal vasculature in the diseased region.

For the CSC subject, we examined the disease features in the FA and ICGA images in more detail. Figure 8 shows the images zoomed into the diseased region. The TopCon images are shown on the left, and the mLSO images are shown on the right. The top row presents the FA images, and the bottom row consists of the ICGA images. The features resolved in both are indicated by white arrows while the features resolved in the TopCon but not the mLSO are indicated by black arrows. The mLSO was able to resolve all the fine features of the disease areas of hyper- and hypo-fluorescence and many of the small capillaries. It could not resolve some of the finest capillaries, as expected due to the resolution of the camera. The mLSO ICGA images show higher contrast imaging of the choroidal vessels from rejection of scattered light and resolution of nearly all of the same disease features.

A subject with diabetic retinopathy (DR) was imaged first on the TopCon and then on the mLSO. Although the subject was imaged at different time points, we were able to assemble comparisons at similar times for the early, mid-, and late phase of the dye infusion. Figure 9 shows the FA images that were collected. The multiple lesions around the arcades on the nasal side of the disc were caused by previous laser treatments. The mLSO
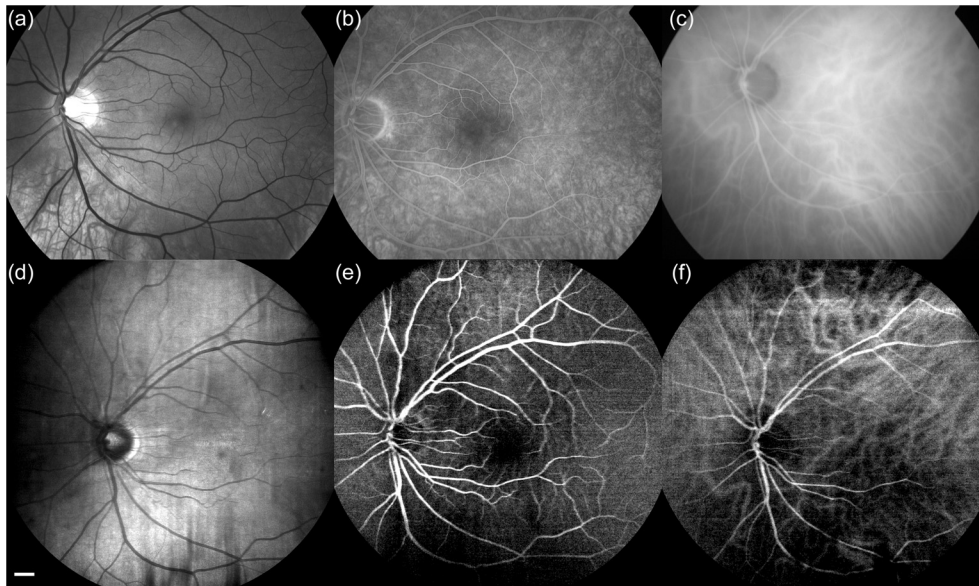
Fig. 6 Comparison of single fundus and fluorescence images from a human subject without retinal disease. Top row (a) to (c): Images from TopCon fundus photography system. Bottom row (d) to (f): Images from mLSO system. (a) Red-free image. (b) Late-phase FA image (04:06 after injection of dye). (c) Late-phase ICGA image. (d) LSO confocal reflectance image. (e) Early-phase FA image (00:46). (f) Early-phase ICGA image (00:48). Scale bar = 3 deg. Field of view is ~50 deg for both imagers. (Video 3, MOV, Quicktime, 15.7 MB) [URL: http://dx.doi.org/10.1117/1.JBO.17.2 .026008.3] shows raw FA video for entire dye infusion cycle corresponding to (e). (Video 4 MOV, Quicktime, 14.2 MB) [URL: http://dx.doi.org/ 10.1117/1.JBO.17.2.026008.4] shows FA frames extracted from Video 3.
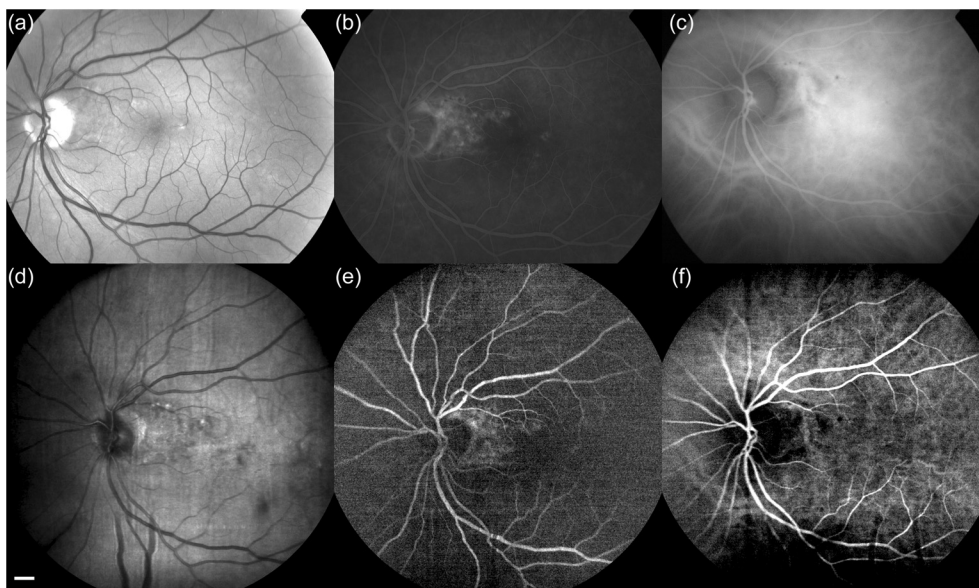
Fig. 7 Comparison of single fundus and fluorescence images from a human subject with stable central serous chorioretinopathy (CSC). Top row (a) to (c): Images from TopCon fundus photography system. Bottom row (d) to (f): Images from mLSO system. (a) Red-free image. (b) Late-phase FA image. (c) Late-phase ICGA image. (d) LSO confocal reflectance image. (e) Early-phase FA image (01:02). (f) Early-phase ICGA image (00:39). Scale bar = 3 deg. Field of view is ~50 deg for both imagers. (Video 5, MOV, Quicktime, 18.2 MB) [URL: http://dx.doi.org/10.1117/1.JBO.17.2 .026008.5] shows entire dye infusion cycle corresponding to (f).

images show good resolution of dye, including late-phase leakage in lesions between the fovea and the disc.

A detail comparison of the early phase images in a region with multiple laser lesions just superior to the fovea is shown in Fig. 10. The detail is labeled similar to Fig. 8. The mLSO imager resolved the same areas of hypo- and hyper-fluorescence in the laser lesions and nearly all the same capillaries as the Top-Con system. It can be misleading to attempt quantitative comparisons of angiography images between the two very different imagers, especially in this case, where the images were collected at different times after dye infusion. However, some quantitative information can be gained by comparison of line profiles across a small capillary as shown in Fig. 10(c). While both imagers were able to resolve this vessel (width of 2 pixels for both), the background noise floor for the TopCon imager was smoother, indicating a higher signal-to-noise ratio (SNR). The standard deviation of 20 pixels immediately surrounding the peak was 3.3 for the TopCon, compared to 9.8 for the
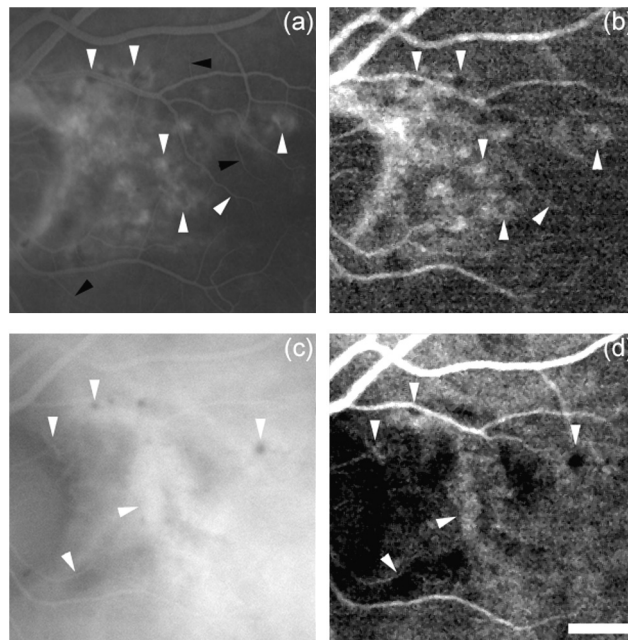
Fig. 8 Detailed comparison of FA and ICGA images from TopCon and mLSO imager in the region of CSC lesions. (a) TopCon FA image. (b) mLSO FA image. (c) TopCon ICGA image. (d) mLSO ICGA image. White arrowheads indicate features (capillaries, hypo-pigmentation, hyper-pigmentation) resolved in both imagers. Black arrowheads indicate features (primarily the smallest capillaries) resolved in the TopCon imager but not the mLSO. Scale bar = 3 deg.
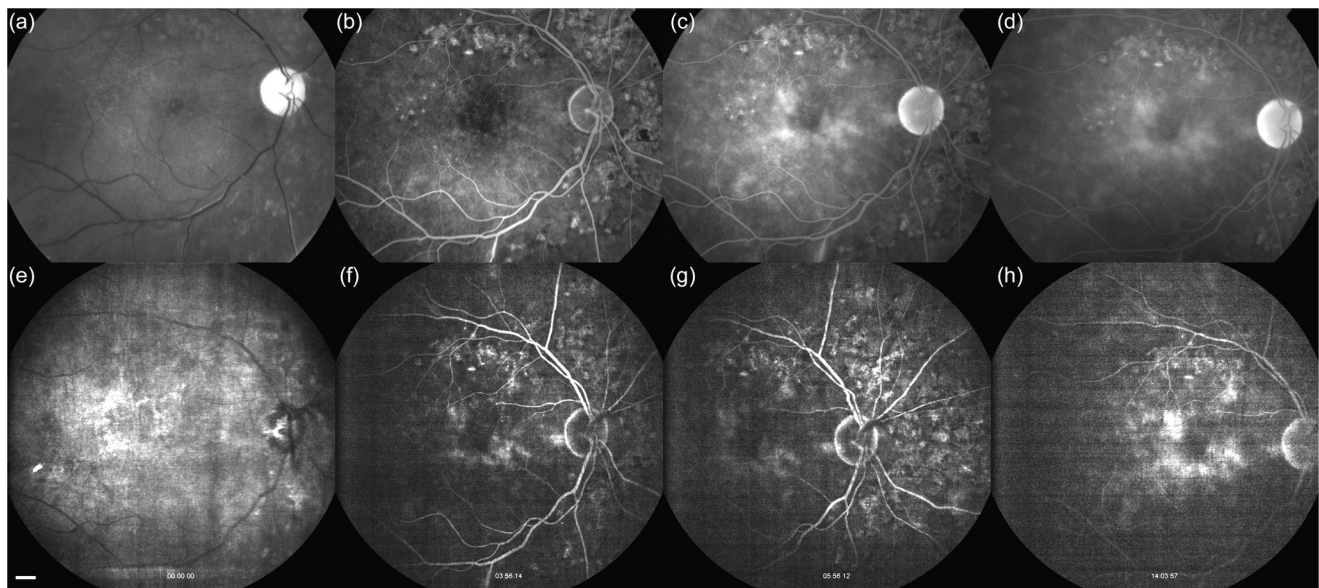

Fig. 9 Comparison of single fundus and FA images at several time points after dye infusion in a human subject with diabetic retinopathy and macular edema. Top row (a) to (d): Images from TopCon fundus photography system. Bottom row (e) to (h): Images from mLSO system. (a) Red-free image. (b) Early-phase FA image (01:30). (c) Mid-phase FA image (09:23). (d) Late-phase FA image (17:32). (e) LSO confocal reflectance image. (f) Early-phase FA image (03:56). (g) Mid-phase FA image (05:56). (h) Late-phase FA image (14:04). Scale bar = 3 deg.

mLSO. The vessel contrast (difference between peak and floor) was slightly higher in the mLSO (68.6 versus 45.8). However, this analysis was done on processed images. A more informative comparison performed on the raw output was not possible because the raw output from the TopCon was not accessible.

The subject with sickle cell retinopathy was imaged first on the TopCon and then on the mLSO (Fig. 11). This subject had a normal macula but large peripheral lesions. We were able to compare images from the mLSO and TopCon at similar points.

Extremely large hyper-fluorescence from dye leakage was seen in the late-phase angiograms.

One of the powerful features of the mLSO is the ability to merge the reflectance, FA, and ICGA images to obtain a more clear picture of ocular health. In a future design, this could be presented to a clinician in real-time with multiple sensors. Figure 12 shows pseudo-color maps for two subjects (without disease and with CSC) generated by merging the gray-scale images from FA and ICGA modes into the green (G) and
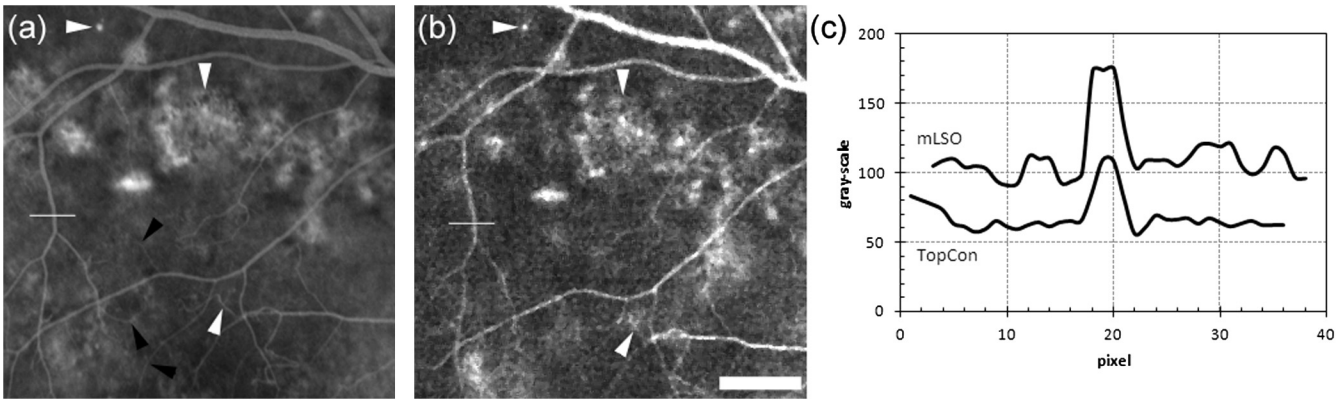
Fig. 10 Detailed comparison of FA and ICGA images from TopCon and mLSO imager in the superior macula in a subject with DR. (a) TopCon FA image. (b) mLSO FA image. (c) Line profiles across capillary on the left side of the images. White arrowheads indicate features resolved in both imagers. Black arrowheads indicate features resolved in the TopCon imager but not the mLSO. Scale bar = 3 deg.
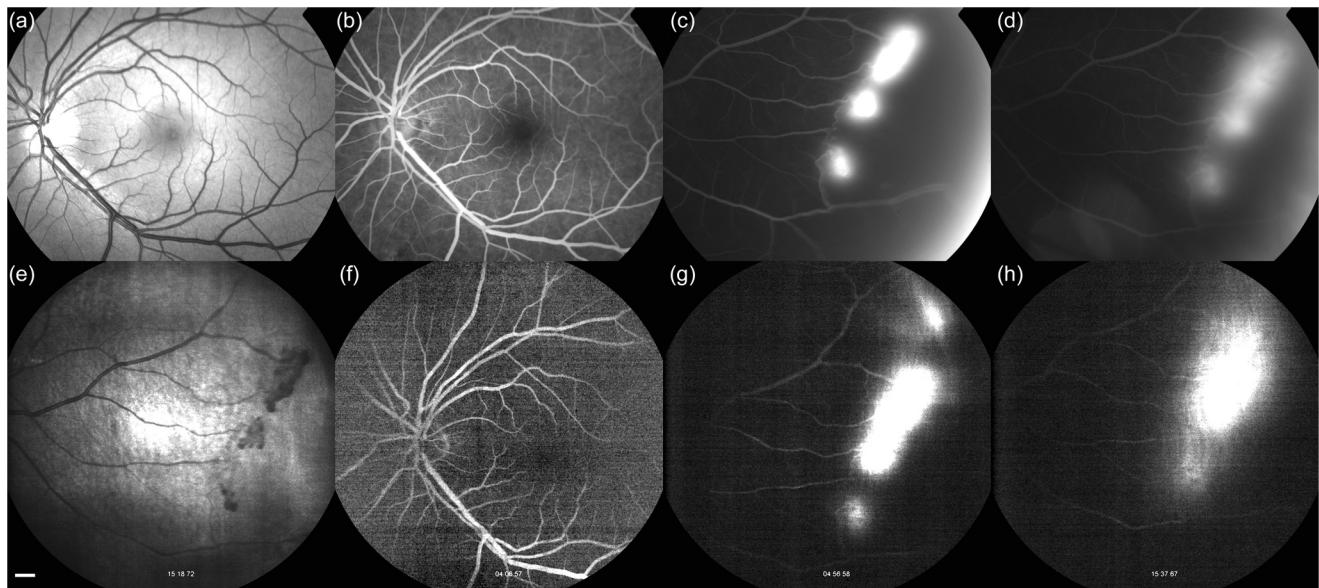

Fig. 11 Comparison of single fundus and FA images in a subject with sickle cell retinopathy. Top row (a) to (d): Images from TopCon fundus photography system. Bottom row (e) to (h): Images from mLSO system. (a) Red-free image. (b) FA image of normal macula (00:54). (c) FA image of peripheral lesions (02:29). (d) Late-phase FA image of peripheral lesions (06:42). (e) LSO confocal reflectance image of peripheral lesions. (f) FA image of normal macula (04:07). (g) FA image of peripheral lesions (04:57). (h) Late-phase FA image of peripheral lesions (15:38). Scale bar = 3 deg.

blue (B) planes of a color image. The merged FA and ICGA image delineates the retinal and choroidal vasculature nicely and enhances disease visualization in the CSC subject. We also added the reflectance image in the red plane (not shown), which distinguished between the disc margin, the scleral crescent, and the lesions in the CSC eye, but did not contribute further information in the eye without disease.

4 Discussion

The pilot clinical investigation is the first demonstration of the ability of the mLSO system to acquire images in FA and ICGA modes using the line field technique. The resolution of the current mLSO implementation is less than the TopCon but is line-camera dependent. When the mLSO imaging was sub-optimal, it had to do with ocular media opacities, patient complications (incomplete dye injection, excessive head or eye movements at the initial mLSO frame, etc.), or the fact that, by design, the mLSO imaging in all but two subjects occurred several minutes

after dye infusion, when the fluorescence signal strength was already significantly diminished. Also, because the mLSO system uses a different principle of operation than the TopCon (confocal versus flood illumination and detection), the appearance of the images was expected to differ between the images irrespective of the mLSO system characteristics or angiography capabilities. The most significant consequence of confocality was the depth sectioning qualities of the imagers, which manifest in the appearance of the very late phase images: the flash-illuminated TopCon collects very low levels of light from all depth layers of the eye to form an image while the mLSO drops below its detection threshold. For this reason, without improved detection and enhanced real-time averaging schemes, the initial mLSO performance in the late phase is not yet at the image quality level of conventional clinical imagers. When these issues are addressed, instruments based on the LSA technique will benefit from a number of natural advantages, including optical path simplicity, compactness, lower cost hardware with efficiently unified
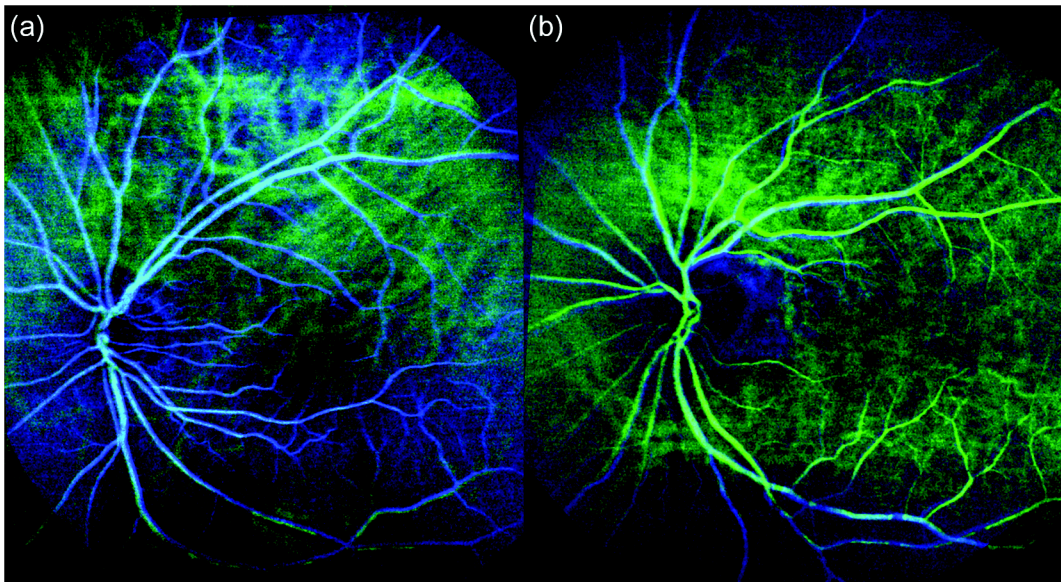
Fig. 12 Pseudo-color images created by merging FA and ICGA images from mLSO for two subjects with: (a) No retinal disease and (b) CSC. Color planes: R: none, G: ICGA, B: FA.

modalities, variable image speed, and novel LSO-based stabilization, registration, and averaging capabilities.

The line scanning angiography approach is fundamentally different from confocal SLO and non-confocal fundus imagers in many ways. In general, flash fundus photography (e.g., Top-Con) floods the eye with illumination light and detects all back-scattered light that returns to the sensor. The optical setup can be relatively simple, consisting of excitation and emission filters, a white light source (Xe arc lamp or similar), and a two-dimensional CCD sensor using a customary indirect ophthalmoscope arrangement that limits the corneal reflex. It is a non-confocal technique, which means that it has no depth-sectioning capability. For angiography, this is less of a concern because the dye is typically confined to specific vascular layers, although separation of retinal and choroidal flow cannot be accomplished. Fundus photography is the gold standard for angiography and produces images with the best resolution; however, it does not produce a continuous sequence of images. The inability to obtain a dynamic record of dye infusion is not often relevant for the majority of clinical diseases but may be important for occlusions, some research applications, and some new therapies.

Confocal scanning laser ophthalmoscopy (e.g., Heidelberg Engineering HRA or Spectralis) is rapidly becoming a clinical standard for imaging. This is primarily because it can accommodate multimodal designs, such as the Spectralis, which is able to obtain red-free, autofluorescence (AF), fluorescein and ICG angiography, and OCT images from a subject in a single session. SLO images are confocal, and so back-scattered light from adjacent voxels are rejected by the pinhole, which can be variably sized according to the endogenous or exogenous fluorophore collection efficiency. The optical setup is generally more complex, but Heidelberg's instruments are generally quite compact. The resolution of the images is lower compared to the TopCon, yet it is able to acquire images continuously.

The mLSO is meant to operate in a similar fashion as an SLO, but with a less complex optical arrangement without a resonant scanner or spinning polygon. It can collect images continuously (e.g., in a video format), all be it at a relatively slow rate compared to normal NIR imaging (1 to 2 fps versus 15 to 60 fps), and it is quasi-confocal and therefore rejects light from voxels (and especially planes) away from the imaging plane. For angiography, this can help distinguish retinal and choroidal features. The mLSO fans the light to a line on the retina and uses a linear sensor for detection in a confocal configuration. The pixel, as opposed to the pinhole in an SLO, produces the confocality. In the axis adjacent to the line, the size is usually much smaller than an SLO pinhole (14 μm versus 100 μm). In the axis along the line, there is reduced confocality. Thus, the mLSO is termed "line confocal" or "quasi-confocal." The LSO (absent optical retinal tracking) has only one moving part, the image scanner, and thus can be made less complex and less costly than a typical SLO. Also, the digital linear detector is usually easier to configure than the analog photomultiplier tube (PMT) or avalanche photodiode (APD) used in an SLO. While the LSO has been shown to produce NIR fundus images that are nearly equivalent to the SLO, it has never been configured for angiography until this study. Because of the fixed pixel size, the light collection properties cannot be controlled as easily as an SLO, which can use a different-sized pinhole to allow more light into the detector. The LSO is operated in a hyper-confocal regime due to the need to trade resolution and sensitivity. In this study, we used a new detector with an asymmetric pixel (14 μm by 28 μm) to enhance the light collection capabilities necessary for angiography (and possibly also AF in the future). Other cameras have parallel sensors that can be binned in the vertical direction adjacent to the line with a variety of (temporal) modes to accomplish a similar result. However, the asymmetric pixel leads to a slight loss of confocality. The results suggest we could have used detectors with a larger ratio in pixel dimensions. The mLSO has lower resolution than the TopCon but can be configured in the future with a higher pixel density. Ultimately, ocular aberrations limit the lateral resolution, and a higher pixel density does not translate to a higher resolution. Other classes of linear detectors have been introduced that

may substantially address the mLSO limitations and are being evaluated for future use.

Although successful for this proof-of-principle investigation, the present mLSO design is far from optimal. Future designs will include multiple line sensors in unique arrangements with peaks centered on the proper emission curves for reflectance, FA, ICGA, and autofluorescence (AF). (The current sensor has a peak quantum efficiency at ∼750 nm.) This adjustment will allow simultaneous acquisition in three imaging modes and real-time color or pseudo-color presentation. It will also allow simultaneous collection of highly confocal NIR LSO reflectance images with a traditional square pixel and FA, ICGA, and AF images with asymmetric pixels. The multi-sensor design need not add significant complexity to the optics. In a previously reported LSO, we used two sensors for stereoscopic retinal views with a common optical path.[13] It may also be possible to improve light sensitivity with nascent avalanche photodiode (APD) or electron multiplied CCD (EMCCD) linear sensor technologies. Other instrumentation enhancements can improve diagnosis and treatment automation procedures.

The goal of the study was to develop a multifunctional system for automated treatment and diagnosis, which also involved significant improvements in the software platform for image acquisition, processing, and post-processing analysis. The integration of modes into a pseudo-color map is one example whereby diagnostic information can be more efficiently presented to the clinician. We also developed several automated analysis programs, including one that automatically and rapidly sizes and demarcates lesions between angiography and laser surgery delivery. In preliminary measurements on existing angiograms, lesion sizing differed by less than 15% between the fully automated algorithm and an ophthalmologist with expertise at laser surgery and lesion identification.[16] Such software enhancements are important for the mLSO-based automated diagnostic and treatment platform.

5 Conclusion

We have successfully developed and built a compact, multifunctional retinal imager that can acquire wide-field, confocal reflectance, indocyanine green and fluorescein angiography images, and deliver PDT therapeutic beams. The system was tested in a multipart human subject investigation at PSI and BUMC. These studies demonstrated all of the key features of the system. The mLSO system will enable researchers and clinicians to image human and animal eyes with a variety of modalities and deliver therapeutic beams from a single interface. These developments may lead to improved patient comfort and reduced imaging session times, allowing clinicians to better diagnose, plan, and conduct patient procedures and also potentially improve outcomes.

References

1. P. J. Rosenfeld et al., "Ranibizumab for neovascular age-related macular degeneration," *N. Engl. J. Med.* **355**(14), 1419–1431 (2006).
2. D. F. Martin et al., "Ranibizumab and bevacizumab for neovascular age-related macular degeneration," *N. Engl. J. Med.* **364**(20), 1897–1908 (2011).
3. TAP Study Group, "Photodynamic therapy of subfoveal choroidal neovascularisation in age-related macular degeneration with verteporfin. One-year results of 2 randomised clinical trials—TAP report 1," *Arch. Ophthalmol.* **117**(10), 1329–1345 (1999).
4. D. M. Brown et al., "Ranibizumab versus verteporfin for neovascular age-related macular degeneration," *N. Engl. J. Med.* **355**(14), 1432–1444 (2006).
5. P. K. Kaiser, "Combination therapy with verteporfin and anti-VEGF agents in neovascular age-related macular degeneration: where do we stand?," *Br. J. Ophthalmol.* **94**(2), 143–145 (2010).
6. A. H. Rogers and A. Witkin, "Neovascular age-related macular degeneration," in *Retinal Imaging* D. Huang et al., eds., Elsevier Inc., Philadelphia pp. 152–163 (2006).
7. D. X. Hammer et al., "Image stabilization for scanning laser ophthalmoscopy," *Opt. Express* **10**(26), 1542–1549 (2002).
8. D. X. Hammer et al., "Compact scanning laser ophthalmoscope with high-speed retinal tracker," *Appl. Opt.* **42**(22), 4621–4632 (2003).
9. R. D. Ferguson et al., "Tracking optical coherence tomography," *Opt. Lett.* **29**(18), 2139–2141 (2004).
10. D. X. Hammer et al., "Adaptive optics scanning laser ophthalmoscope for stabilized retinal imaging," *Opt. Express* **14**(8), 3354–3367 (2006).
11. S. A. Burns et al., "Large field of view, modular, stabilized, adaptive-optics-based scanning laser ophthalmoscope," *J. Opt. Soc. Am. A* **24**(5), 1313–1326 (2007).
12. R. D. Ferguson et al., "Adaptive optics SLO with integrated wide-field retinal imaging and tracking," *J. Opt. Soc. Am. A* **27**(11), A265–A277 (2010).
13. D. X. Hammer et al., "Line-scanning laser ophthalmoscope," *J. Biomed. Opt.* **11**(4), 041126 (2006).
14. R. D. Ferguson et al., "Wide-field retinal hemodynamic imaging with the tracking scanning laser ophthalmoscope," *Opt. Express* **12**(21), 5198–5208 (2004).
15. G. Maguluri et al., "Three-dimensional tracking for volumetric spectral-domain optical coherence tomography," *Opt. Express* **15**(25), 16808–16817 (2007).
16. D. X. Hammer et al., "Multimodal scanning laser ophthalmoscopy for image guided treatment of age-related macular degeneration," *Proc. SPIE* **7163**, 71631C (2009).